Biochimica et Biophysica Acta 1818 (2012) 2260–2270

Contents lists available at SciVerse ScienceDirect

Biochimica et Biophysica Acta

journal homepage: www.elsevier.com/locate/bbamem

Human erythrocytes and neuroblastoma cells are *in vitro* affected by sodium orthovanadate

M. Suwalsky [a,*], P. Fierro [a], F. Villena [b], L.F. Aguilar [c], C.P. Sotomayor [c], M. Jemiola-Rzeminska [d], K. Strzalka [d], S. Gul-Hinc [e], A. Ronowska [e], A. Szutowicz [e]

[a] Faculty of Chemical Sciences, University of Concepción, PO Box 160-C, Concepción, Chile
[b] Faculty of Biological Sciences, University of Concepción, Concepción, Chile
[c] Instituto de Química, Pontificia Universidad Católica de Valparaíso, Valparaíso, Chile
[d] Department of Plant Physiology and Biochemistry, Faculty of Biochemistry, Biophysics and Biotechnology, Jagiellonian University, Krakow, Poland
[e] Chair of Clinical Biochemistry, Department of Laboratory Medicine, Medical University of Gdansk, Debinki 7, 80-211, Gdansk, Poland

ARTICLE INFO

Article history:
Received 26 January 2012
Received in revised form 29 March 2012
Accepted 16 April 2012
Available online 21 April 2012

Keywords:
Orthovanadate
Erythrocyte membrane
Lipid bilayer
Neuroblastoma cell

ABSTRACT

Research on biological influence of vanadium has gained major importance because it exerts potent toxic, mutagenic, and genotoxic effects on a wide variety of biological systems. However, hematological toxicity is one of the less studied effects. The lack of information on this issue prompted us to study the structural effects induced on the human erythrocyte membrane by vanadium (V). Sodium orthovanadate was incubated with intact erythrocytes, isolated unsealed human erythrocyte membranes (IUM) and molecular models of the erythrocyte membrane. The latter consisted of bilayers of dimyristoylphosphatidylcholine (DMPC) and dimyristoylphosphatidylethanolamine (DMPE), phospholipid classes located in the outer and inner monolayers of the human erythrocyte membrane, respectively. This report presents evidence in order that orthovanadate interacted with red cell membranes as follows: a) in scanning electron microscopy (SEM) studies it was observed that morphological changes on human erythrocytes were induced; b) fluorescence spectroscopy experiments in isolated unsealed human erythrocyte membranes (IUM) showed that an increase in the molecular dynamics and/or water content at the shallow depth of the lipids glycerol backbone at concentrations as low as 50 μM was produced; c) X-ray diffraction studies showed that orthovanadate 0.25–1 mM range induced increasing structural perturbation to DMPE; d) somewhat similar effects were observed by differential scanning calorimetry (DSC) with the exception of the fact that DMPC pretransition was shown to be affected; and e) fluorescence spectroscopy experiments performed in DMPC large unilamellar vesicles (LUV) showed that at very low concentrations induced changes in DPH fluorescence anisotropy at 18 °C. Additional experiments were performed in mice cholinergic neuroblastoma SN56 cells; a statistically significant decrease of cell viability was observed on orthovanadate in low or moderate concentrations.

1. Introduction

Vanadium is widely distributed in the environment as well as in biological systems, and it is also a major trace element in fossil fuels. Consequently, combustion of these materials represents a significant source of vanadium into the environment. Vanadium is a transition metal, which is possible to be found in the (III), (IV) and (V) oxidation states. Although most foods contain low concentrations of vanadium, food itself is the major source of exposure for the general population. The estimated daily intake of the U.S. population ranges from 10 to 60 μg [1]. In most of the foods, physiologically relevant forms of vanadium include vanadyl sulfate, sodium metavanadate, sodium orthovanadate and vanadium pentoxide [2]. The (V) state, as vanadate, predominates in extracellular body fluids whereas the (IV) state is the most common intracellular form. However, vanadates such as orthovanadate, decavanadate, metavanadate anions and vanadyl cations are interconverted in aqueous solutions depending on concentration, pH and the state of redox potential [3]. Research on biological influence of vanadium has gained major importance because it is well known that it exerts potent toxic, mutagenic, and genotoxic effects on a wide variety of biological systems [4,5]. Under physiological conditions, both (IV) and (V) oxidation states of vanadium are accessible both kinetically and thermodynamically. So the shuttle between these two oxidation states may play a pivotal role in the biological effects of

Abbreviations: SEM, scanning electron microscopy; IUM, isolated unsealed human erythrocyte membrane; LUV, large unilamellar vesicles; r, anisotropy; GP, generalized polarization; DPH, 1,6-diphenyl-1,3,5-hexatriene; laurdan, 6-dodecanoyl-2-methylaminonaphthalene; DMPC, dimyristoylphosphatidylcholine; DMPE, dimyristoylphosphatidylethanolamine; PDH, pyruvate dehydrogenase; ChAT, choline acetyltransferase; cAMP, dibutyryl cAMP; DC, differentiated cells; NC, nondifferentiated cells; RA, all trans retinoic acid

* Corresponding author. Tel.: +56 41 2204171; fax: +56 41 2245974.
E-mail address: msuwalsk@udec.cl (M. Suwalsky).

0005-2736/$ – see front matter © 2012 Elsevier B.V. All rights reserved.
doi:10.1016/j.bbamem.2012.04.012

vanadium compounds. However, there are only limited data available on the redox stability and interconversion among oxidation states of vanadium in biological media [6]. It has been shown that intracellular vanadate is readily reduced by cytoplasmic glutathione and essentially all the vanadium is present in the (IV) form [7]. Vanadium compounds have been shown to inhibit Na^+,K^+ -ATPase, acid and alkaline phosphatase, adenyl kinase as well as several of the enzymes in the glycolytic pathway. Since vanadate can adopt a stable trigonal bipyramidal structure that resembles phosphates, it could inhibit enzyme activity by replacing phosphate as a substrate [7,8].

Despite the well documented information, there is a lack of reports concerning the effects of vanadium compounds on both structure and functions of cell membranes, particularly those of human erythrocytes. It has been reported that sodium orthovanadate and metavanadate promoted a significant lowering of red blood cell count [9,10], reduced the deformability of erythrocytes and produced peroxidative changes in the erythrocyte membrane leading to hemolysis [11]; therefore, the depressed erythrocyte count in vanadium intoxicated animals may be the consequence of both hemolytic action of vanadium and the shortened time of erythrocyte survival [11]. Vanadate also inhibited the stomatocytic shape change produced by amphipathic cationic drugs, but not that induced by low pH [8].

The most important function of any biological membrane is to serve as a general diffusion barrier. Therefore, its structure and functions are susceptible to alterations as a consequence of interactions with chemical species. With the aim to better understand the molecular mechanisms of the interaction of vanadium with cell membranes we have utilized human erythrocytes and molecular models of the erythrocyte membranes. Erythrocytes were chosen because although less specialized than many other cell membranes they carry on enough functions in common with them such as active and passive transport, as well as the production of ionic and electric gradients, to be considered representative of the plasma membrane in general. Molecular models consisted of bilayers of dimyristoylphosphatidylcholine (DMPC) and dimyristoylphosphatidylethanolamine (DMPE), representative of phospholipid classes located in the outer and inner monolayers of the human erythrocyte membrane, respectively [12,13]. The capacity of orthovanadate to perturb the multibilayer structures of DMPC and DMPE was evaluated by X-ray diffraction and differential scanning calorimetry (DSC) while DMPC unilamellar vesicles (LUV) were studied by fluorescence spectroscopy. In an attempt to further elucidate their effects on cell membranes, the present work also examined their influence on the morphology of intact human erythrocytes by scanning electron microscopy (SEM), while isolated unsealed human erythrocyte membranes (IUM) were studied by fluorescence spectroscopy. These systems and techniques have been used in our laboratories to determine the interaction with and the membrane-perturbing effects of other inorganic compounds [14–16].

Although RBCs are a convenient model for studying vanadium–biological membrane interactions, they are not suitable for investigation of the majority of metal-induced metabolic and cytotoxic effects due to the lack of key intracellular organelles. On the other hand, neuronal cells are known to be particularly susceptible to several endogenous and exogenous metals due to their high demand for energy supply [17]. As vanadium species are considered as potential complementary anti-diabetic compounds, its potential acute and chronic neurotoxicity becomes a key issue [4,18,19]. However, reports on vanadium effects in the central nervous system are scarce and conflicting. It has been shown that vanadium pentoxide exerted dopaminergic neurotoxicity in cellular models of Parkinson's disease [20]. It has also been reported that vanadium-organic cyclic compounds displayed neuroprotective properties on cholinergic *in vivo* neurons in ischemic or stereotactically injured brains [21,22]. Due to concerns on possible neurotoxic effects of environmentally introduced vanadium its influence on clonal cholinergic cells originating from mice septum was also investigated.

2. Materials and methods

2.1. X-ray diffraction studies of phospholipid multilayers

The capacity of orthovanadate to perturb the structures of DMPC and DMPE multilayers was evaluated by X-ray diffraction. Synthetic DMPC (lot 140PC-224, MW 677.9), DMPE (lot 140PC-230, MW 635.9) from Avanti Polar Lipids (AL, USA); and Na_3VO_4 from Sigma-Aldrich (St. Louis, MO, USA) were used without further purification. About 2 mg of each phospholipid was introduced into 1.5 mm diameter special glass capillaries, which were then filled with 200 μl of (a) distilled water and (b) aqueous solutions of Na_3VO_4 in a range of concentrations (0.25 mM to 50 mM). Specimens were X-ray diffracted after 1 h incubation at 37 °C and 60 °C with DMPC and DMPE, respectively, in flat plate cameras. Specimen-to-film distances were 8 and 14 cm, standardized by sprinkling calcite powder on the capillary surface. Ni-filtered CuKα radiation from a Bruker Kristalloflex 760 (Karlsruhe, Germany) X-ray generator was used. The relative reflection intensities were obtained in a MBraun PSD-50M linear position-sensitive detector system (Garching, Germany); no correction factors were applied. Experiments were performed at 19 ± 1 °C, which is below the main phase transition temperature of both DMPC and DMPE. Higher temperatures would have induced lipid transitions to more fluid phases making it very difficult to detect structural changes. Each experiment was repeated three times and in case of doubts additional experiments were carried out.

2.2. Differential scanning calorimetry (DSC) studies of phospholipid multilamellar liposomes (MLV)

Appropriate amounts of lipids (DMPC, lot 049H5156 and DMPE, lot 13H83681) from Sigma dissolved in chloroform were evaporated under gaseous nitrogen to form a thin film on the glass test tube walls. In order to remove the remnants of moisture, samples were subsequently exposed to vacuum for 1 h. Dry lipid films were suspended in buffer (1 mM EDTA/10 mM Hepes/50 mM KCl, pH 7.7), and aqueous solutions of orthovanadate were added in the concentration range of 0.25 mM to 1 mM. The multilamellar liposomes (MLV) were prepared by vortexing the samples at the temperature above gel-to-liquid crystalline phase transition of the pure lipid (about 30 °C for DMPC and 60 °C for DMPE). The DSC measurements were performed using a differential scanning calorimeter (CSC 6100 Nano II, Calorimetry Sciences Corp., Provo, UT, USA). To avoid bubble formation during heating modes the samples were degassed prior to loading by putting the vacuum of 0.3–0.5 atm on the solution for 10 min. Then the sample cell was filled with about 400 μl of MLV suspension and an equal volume of buffer itself was used as a reference. Cells were sealed and equilibrated for about 20 min below starting temperature of the run. The scan range was 5–40 °C for DMPC and 30–70 °C for DMPE. Heating/cooling scan rates were 1 °C per minute. The heating scans were carried out first. The reference scan was subtracted from the sample scan and each data set was analyzed for the thermodynamic parameters with CPCALC software package supplied by CSC (Provo, UT, USA). The accuracy for the main phase transition temperature and enthalpy was ± 0.1 °C and ± 0.8 kJ/mol, respectively.

2.3. Fluorescence measurements of DMPC large unilamellar vesicles (LUV) and isolated unsealed human erythrocyte membranes (IUM)

The effects of orthovanadate upon the physicochemical properties of isolated unsealed erythrocyte membranes and DMPC large unilamellar vesicles were evaluated through steady state and time resolved fluorescence spectroscopy. A non-polar membrane probe DPH was used to examine the hydrophobic deep domains of the corresponding lamellae. Due to its hindered rotation in ordered

lamellae its steady-state fluorescence anisotropy measurements provide information related to the lipid acyl chain packing order. DPH fluorescence lifetime, obtained from time resolved fluorescence decay data provides information about the polarity, and hence the hydration degree in the mentioned lamella domains. The amphiphilic probe laurdan, was used to examine the polarity and/or molecular dynamics in the hydrophobic–hydrophilic interface at the lipid glycerol backbone level. The generalized polarization (GP) concept was used to quantify laurdan large fluorescence spectral shift [23].

Steady-state and time-resolved fluorescence measurements were performed in a phase shift and modulation K2 spectrofluorometer (ISS, Inc., Champaign, IL, USA). For both probes, the exciting light originated from an ISS modulable 375 nm LED laser. Software from ISS was used for both data collection and analysis. LUV suspension measurements were carried out at 18 °C and 37 °C, and IUM measurements were performed at 37 °C using 5 mm path-length square quartz cuvettes. Anisotropy measurements were made in the L configuration using Glan Thompson prism polarizers in both exciting and emitting beams. The emission was measured using a WG-420 Schott high-pass filter (Mainz, Germany) with negligible fluorescence. DPH fluorescence anisotropy (r) was calculated according to the definition: $r = (I_{||} - I_{\perp}) / (I_{||} + 2I_{\perp})$, where $I_{||}$ and $I_{\perp}$ are the corresponding vertical and horizontal emission fluorescence intensities with respect to the vertically polarized excitation light [24]. Laurdan fluorescence spectral shifts were quantitatively evaluated through the GP concept which is defined by the expression $GP = (I_b - I_r) / (I_b + I_r)$, where I_b and I_r are the emission intensities at the blue and red edges of the emission spectrum, respectively. These intensities have been measured at the emission wavelengths of 440 and 490 nm, corresponding to the emission maxima of laurdan in both gel and liquid crystalline phases, respectively [25]. Lifetime measurements were carried out with the polarizers oriented in the "magic angle" condition [26]. Phase and modulation values were obtained at 10 modulation frequencies (5–100 MHz) as previously described [27]. Dimethyl-POPOP (1,4-bis [2]4-methyl-5-phenyloxazoly-benzene) in ethanol ($\tau = 1.45$ ns) was used as a reference of intensity decay. Time-resolved fluorescence intensity decay data of DPH was analyzed using a Lorentzian lifetime distribution. A fixed discrete lifetime component of 0.01 ns was used to account for scattered light, which was <2% in terms of fractional intensity contribution. The Lorentzian lifetime distribution center obtained from the analysis is informed as DPH lifetime.

DMPC LUV suspended in water were prepared by extrusion of frozen and thawed multilamellar liposome suspensions (final lipid concentration 0.4 mM) through two stacked polycarbonate filters of 400 nm pore size (Nucleopore, Corning Costar Corp., MA, USA) under nitrogen pressure at 10 °C above the lipid phase transition temperature. Erythrocytes were separated from heparinized venous blood samples obtained from normal casual donors by centrifugation and washing procedures. IUM were prepared by lysis, according to Dodge [28]. DPH and laurdan were incorporated into LUV and IUM by addition of 2 μl/ml aliquots of 0.5 mM solutions of the probe in dimethylsulfoxide and ethanol, respectively, in order to obtain final analytical concentrations of 1 μM, and incubated them at 37 °C for 45 min. Sample temperature was controlled by an external bath circulator (Cole-Parmer, Chicago, IL, USA) and monitored before and after each measurement using an Omega digital thermometer (Omega Engineering, Inc., Stanford, CT, USA). Na_3VO_4 was incorporated in LUV and IUM suspensions by addition of adequate (ca. 0.1 M) aliquots of aqueous solution in order to obtain the different concentrations used in this work. Samples thus prepared were then incubated at 37 °C for ca. 15 min. Blank subtraction was performed in all measurements using unlabeled samples without probes. The data represent mean values and standard error of ten measurements in two independent samples. Unpaired Student's t-test was used for statistical calculations.

2.4. Scanning electron microscopy (SEM) studies of human erythrocytes

In vitro interaction of sodium orthovanadate with erythrocytes was attained by incubating red blood cell suspensions derived from healthy human male donors not receiving any pharmacological treatment. Blood samples (0.1 ml) were obtained by puncture of the ear lobule and by aspiration into a tuberculin syringe without needle containing 5000 units/ml heparin in 0.9 ml phosphate buffered saline (PBS), pH 7.4. Red blood cells were then centrifuged for 10 min, washed three times in PBS, resuspended in PBS containing orthovanadate in a range of concentrations and incubated for 1 h at 37 °C. Controls were cells resuspended in PBS without the salts. Specimens were then fixed overnight at 5 °C by adding one drop of each sample to plastic tubes containing 1 ml of 2.5% glutaraldehyde, washed twice in distilled water, placed on siliconized Al stubs, air dried at 37 °C for 30 min and gold coated for 3 min at 13.3 Pa in a sputter device (Edwards S 150, Sussex, England). Specimens were examined in a JEOL (JEM 6380 LB, Japan) SEM. Data were expressed as mean ± standard deviation of 50 cell counts.

2.5. Effects of orthovanadate on viability and acetyl-CoA metabolism of cholinergic SN56 neuroblastoma cells

Unless otherwise specified biochemicals were obtained from Sigma-Aldrich (Poznań, Poland), [1-^{14}C-acetyl]-CoA 4 mCi/mmol was from Perkin-Elmer (Boston, MA, USA), cell culture growth media and components were provided by Gibco Life Technologies (Warsaw, Poland), and cell culture disposables were derived from Sarstedt (Stare Babice, Poland).

2.5.1. Cell cultures

SN56.B5.G4 cholinergic murine neuroblastoma cells, with stable expression of PDH and ChAT between 22–40th passage, were used for experiments [29,30]. Cells were seeded at density of 40,000 cells/cm^2 on 75 cm^2 Falcon vessels in Dulbecco's modified Eagle medium containing 1 mM glutamine, 0.05 mg of streptomycin and 50 U of penicillin per 1 ml and 10% fetal bovine serum (DMEM-FBS) and grown at 37 °C in atmosphere 5% CO_2, 95% air to obtain cell of non-differentiated phenotype (NC). Cells were differentiated by combined addition of 1 mmol/l dibutyryl cAMP (cAMP) and 0.001 mmol/l all-trans-retinoic acid (RA) for 72 h (DC). They were harvested into 10 ml of ice cold 140 mmol/l NaCl containing 5 mmol/l KCl, 1.7 mmol/l NaK-phosphate buffer (pH 7.4) and 5 mM glucose and collected by centrifugation at 200×*g* for 7 min. Supernatant was removed and cells were suspended in 320 mmol/l sucrose containing 10 mmol/l HEPES buffer (pH 7.4) to obtain protein concentration 10.0 mg/ml. Immediately after collection the cells were used for trypan blue exclusion assay and for metabolic studies. For ChAT and PDH assays samples were kept frozen at −20 °C for 2–7 days. Remaining enzyme activities were assessed in unfrozen samples within 24 h after harvesting cells.

2.5.2. Metabolic and viability studies

Depolarizing incubation medium contained in a final volume of 1.0 ml 2.5 mmol/l pyruvate, 2.5 mmol/l L-malate, 90 mmol/l NaCl, 30 mmol/l KCl, 20 mmol/l NaHEPES (pH 7.4), 1.5 mmol/l Na-phosphate, 0.01 mmol/l choline chloride, 0.015 mmol/l eserine sulfate, 32 mmol/l sucrose, Na_3VO_4 in concentrations as indicated, and 0.7–1.0 mg of cell protein. It was used to assure depolarization of the cells to simulate excitotoxic stimulation taking place in different pathologic brain conditions. Incubation was started by the addition of cell suspension and continued for 30 min at 37 °C with shaking at 100 cycles per min. For determination of total acetyl-CoA content, 0.3 ml of incubation medium was centrifuged at 5000×*g* for 2 min. Supernatant was removed and cell pellet was deproteinized as indicated below. For enzyme assays, at the end of incubation, the medium containing cell suspension was

centrifuged for 2 min at 10,000×*g*. Supernatant was discarded and pellet was suspended in a small volume of 320 mM sucrose, homogenized with Teflon pestle microhomogenizer (Sigma, Poznań, Poland), diluted to desired protein concentration with 0.2% w/V Triton X-100 and immediately used for the enzyme assays. Assay media contained no Na_3VO_4 added.

2.5.3. Acetyl-CoA assay

For assaying of whole cell acetyl-CoA content, the cell pellet was deproteinized by suspension in a small volume of 5 mmol/l HCl and incubated in a boiling bath for 1 min. To assess acetyl-CoA content in the cell mitochondria 0.5 ml of incubation medium was mixed with equal volume of lysing solution containing 1.4 mg digitonin/ml in 125 mmol/l KCl with 20 mmol/l NaHEPES buffer (pH 7.4) and 3 mmol/l EDTA. Lysate was transferred on 0.5 ml of silicone oil mixture (AR 20 and AR200, 1:2) layered over 0.1 ml of buffered 320 mM sucrose. After 30 s the mitochondrial fraction was separated from the soluble one by centrifugation for 40 s at 12,000×*g*. After removal of soluble fraction, silicon oils and sucrose, mitochondrial pellet was deproteinized as described above. Deproteinized extracts of whole cells and mitochondria were treated with maleic anhydride solution in ethyl ether for 2 h to remove CoA-SH. Cycling reaction was carried for 60 min in 0.1 ml of medium containing 1.9 mmol/l acetyl phosphate, 1.2 mmol/l oxaloacetate, 1.0 IU phosphotransacetylase and 0.12 IU citrate synthase. Cycling reaction was stopped by heating samples at 100 °C for 10 min and citrate formed was determined [31]. Cytoplasmic acetyl-CoA level was calculated by subtraction of mitochondrial acetyl-CoA from total acetyl-CoA content [31].

2.5.4. Trypan blue exclusion assay

After 30 min incubation cell suspension was mixed with equal volume of 0.4% isotonic trypan blue solution. Total cell number and fraction of nonviable, dye accumulating cells were counted after 2 min in Fuchs-Rosenthal hemocytometer under light microscope [32].

2.5.5. Enzyme assays

Immediately before the assay, samples were diluted until desired protein concentration in 0.2% v/v Triton X-100. Choline acetyltransferase (ChAT, EC 2.3.1.6) activity was assessed by the radiometric method using [1-^{14}C]acetyl-CoA as a substrate [33]. PDH was assayed by the citrate synthase coupled method [34]. Activities of aconitase (1.3.99.1) and NADP-isocitrate dehydrogenase (threo-D-isocitrate:NADP oxidoreductase (decarboxylating), ICDH-NADP, EC 1.1.1.42) were assayed by methods described elsewhere [35,36].

2.5.6. Protein assay

Protein was assayed following the method by Bradford [37] with human immunoglobulin as a standard.

2.5.7. Statistics

Statistical analyses were carried out by one way ANOVA with Bonferroni multiple comparison test or by non-paired Student's *t* test, at $p<0.05$ being considered to be statistically significant.

3. Results

3.1. X-ray diffraction studies of phospholipid multilayers

Fig. 1A exhibits the results obtained by incubating DMPC with water and Na_3VO_4. As expected, water altered the structure of DMPC, as its bilayer repeat (phospholipid bilayer width plus the layer of water) increased from about 55 Å in its dry crystalline form [38] to 65 Å when immersed in water, and its low-angle reflections, (indicated as (LA) in the figure) which correspond to DMPC polar terminal groups, were reduced to only the first two orders of the bilayer width. On the other hand, only one strong reflection of 4.2 Å showed up in the wide-angle region (WA), which corresponds to the average distance between fully extended acyl chains organized with rotational disorder in hexagonal packing. Thus, DMPC showed the typical characteristics of the Pβ′ gel phase. Fig. 1A discloses that after exposure to 20 mM and higher orthovanadate concentrations there was a weakening of the low-angle lipid reflection intensities together with a shift towards higher interplanar spacings. From these results it can be concluded that orthovanadate produced a significant structural perturbation of DMPC bilayers but at relatively high concentrations. Fig. 1B shows the results of the X-ray diffraction analysis of DMPE bilayers incubated with water and Na_3VO_4. As reported elsewhere, water at a temperature below DMPE main transition (about 51 °C) does not significantly affect the bilayer structure in its solid crystalline phase [38]. However, after heating to 60 °C and cooling down to room temperature (*ca. 18 °C*) DMPE was in a liquid crystal phase as its X-ray reflections were reduced to one of 56.4 Å and another of 4.2 Å in the low- and wide-angle regions, respectively. Fig. 1B shows that 0.5 mM orthovanadate induced a significant weakening of DMPE reflection intensities, all of which practically disappeared with 1 mM Na_3VO_4. From these results it can be concluded that orthovanadate induced stronger structural perturbations to DMPE than to DMPC bilayers.

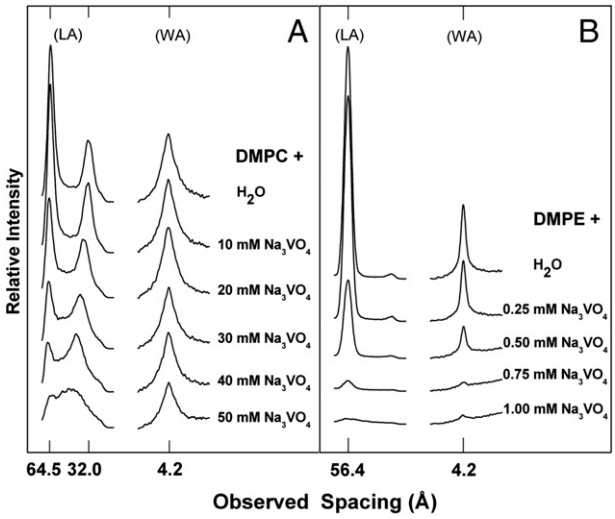

Fig. 1. Microdensitograms from X-ray diffraction diagrams of DMPC and DMPE in water and aqueous solutions of (A, B) sodium orthovanadate; (LA) low-angle and (WA) wide-angle reflections.

3.2. Differential scanning calorimetry (DSC) studies of phospholipid multilamellar liposomes (MLV)

The representative high-sensitivity DSC heating thermograms obtained for pure DMPC multibilayer vesicles and binary mixtures of DMPC and orthovanadate at various concentrations are shown in Fig. 2. In the absence of any additives fully hydrated DMPC bilayers undergo two thermotropic phase transitions in the temperature range from 5 to 40 °C; the highly cooperative main transition ($P_{\beta'} \rightarrow L_\alpha$ phase transition) at 24.4 °C with an enthalpy change (ΔH) of 5.5 kcal mol^{-1}, which corresponds to the gel-to-liquid-crystal transition, and the smaller one ($L_{\beta'} \rightarrow P_{\beta'}$ phase transition) occurring at 14.9 °C with a ΔH of 0.7 kcal mol^{-1}, so called pretransition. Here the transition temperatures correspond to the transition peak at the maximal peak height and the transition enthalpies correspond to the integrated area under the peak divided by the lipid concentration. The results for the thermodynamic data of the pure DMPC are in agreement with previous reports (for reviews see [39–41]). In the case of orthovanadate at the highest concentration under the studies

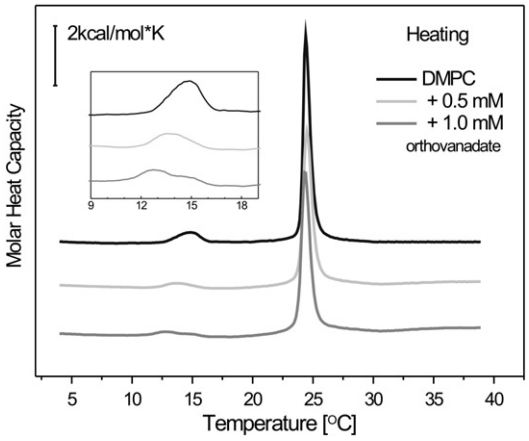

Fig. 2. Representative DSC curves obtained from multilamellar DMPC liposomes containing different orthovanadate concentrations. Scans were obtained at a heating rate of 1 °C min^{-1}.

only a slight downwards shift ($\Delta T = 1$ °C) is observed. Fig. 3 shows the set of representative heating profiles obtained for DMPE liposomes. In the thermal range of 30–70 °C, the pure DMPE bilayers exhibit a strong and sharp main-transition at 50.7 °C, with an enthalpy change (ΔH) of 6.7 kcal mol^{-1}, arising from the conversion of gel to liquid-crystal phase. The transition is reversible and the shape of the peak is roughly symmetrical. Thermodynamical parameters found for DMPE are concurrent with the literature data [42]. Unlike phospholipids containing choline group, DMPE bilayers are affected by the presence of orthovanadate as the phase transition temperature undergoes a shift to the lower values in the concentration-dependent manner. The effectiveness in thermotropic phase transition perturbations exerted by examined compound was further analyzed in terms of thermodynamic parameters. Tables 1 and 2 present values of temperature, enthalpy and entropy for DMPC and DMPE systems, respectively, determined on the basis of heating and cooling scans.

3.3. Fluorescence measurements of DMPC large unilamellar vesicles and isolated unsealed human erythrocyte membranes

The concentration dependent effect of orthovanadate incorporation on the properties of DMPC LUV and IUM was assessed at 18 °C and 37 °C on DMPC LUV and at 37 °C on IUM. DPH steady state fluorescence anisotropy values in DMPC LUV and in IUM, are depicted in Fig. 4, as a function of orthovanadate concentration up to 1 mM. The addition of this compound elicited slight changes in anisotropy parameter; in IUM suspension two local maxima appear upon the addition of 0.1 and 0.5 mM of the additive. In the case of DMPC LUV, in the gel state (18 °C) two small local minima appear upon the addition of 0.05 and 0.8 mM of the additive, while in the liquid crystalline state (37 °C) only very slight variations occurred which resemble that of IUM suspensions. Laurdan's emission spectral shifts, as a function of the additive concentration assessed through the generalized polarization parameter GP, are depicted in Fig. 5. Orthovanadate addition induced a steadily small increase only in DMPC LUV in the liquid crystalline state (37 °C) at concentrations higher than 0.2 mM of the additive. No significant changes were obtained in LUV in the gel state and in IUM. DPH fluorescence lifetime (Fig. 6) shows in IUM slight but significant changes, as a sharp decrease since the first orthovanadate addition, leading to a minimum at 0.01 mM with a subsequent increase, leveling at 0.15 mM of the additive. The very slight changes in DMPC LUV at both temperatures are not considered significant variations.

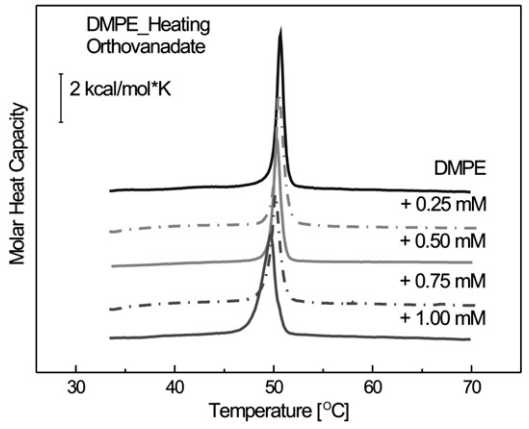

Fig. 3. Representative DSC curves obtained from multilamellar DMPE liposomes containing different orthovanadate concentrations. Scans were obtained at a heating rate of 1 °C min^{-1}.

3.4. Scanning electron microscopy (SEM) studies of human erythrocytes

Fig. 7 shows SEM examinations of human red blood cells incubated with 0.5 mM and 1 mM Na_3VO_4. As it can be appreciated, orthovanadate produced alterations to the normal discoid morphology of the erythrocytes (Fig. 7A). In the case of 0.5 mM Na_3VO_4, almost all the cells exhibit echinocytic deformation, and only a few remain intact (Fig. 7B). In the 1 mM concentration, all the erythrocytes are affected, and the echinocytosis is more marked (Fig. 7C). Higher concentrations (not shown) induced cellular polymorphism; the profiles correspond to echinocytes, stomatocytes, spherostomatocytes, knizocytes, and moreover, all the cells are microcytes.

3.5. Effects of orthovanadate on viability and acetyl-CoA metabolism of cholinergic SN56 neuroblastoma cells

Brain cholinergic neurons are known to be particularly sensitive to several neurodegenerative signals, including overload with endogenous and exogenous metals due to their high demand for acetyl-CoA used by them not only for energy production but also for acetylcholine synthesis [30,43]. Therefore, it is expected that they might be the most sensitive target of putative vanadium neurotoxicity. Nondifferentiated SN56 cholinergic cells (NC) displayed low activity of choline acetyltransferase as well as acetylcholine content and its release rate. Three day culture with 1 mM dibutyryl cAMP and 0.001 mM all-trans-retinoic acid resulted in besides morphological maturation 2–3 fold increase of these cholinergic marker levels in SN56 cells (Figs. 8 and 9A, B). Differentiation caused also 30% inhibition of cell multiplication as evidenced by cell count by the end of the culture (Fig. 10). Orthovanadate, after 30 min exposition, caused disappearance of cell extensions that became round-shaped. Many of them displayed multiple vacuoles and blebs (Fig. 9C, D). Incubation of harvested NC in vanadate free depolarizing medium for 30 min caused no changes in their viability that remained on 97–99% level (Fig. 11). On the other hand, short 30 min exposition of harvested DC to increasing orthovanadate concentrations caused much greater concentration-dependent loss of viability than the NC ones (Fig. 11). Namely 0.005 mmol/l orthovanadate increased fraction of trypan blue positive DC to 12%, without compromising viability of NC (Fig. 11). The increase of orthovanadate concentration to 0.050 mmol/l elevated nonviable fraction of DC to 23% and that of NC to 8% only (Fig. 11). Further increase of Na_3VO_4 to 0.200 mmol/l caused no alteration of nonviable cell fraction. Despite of partial loss of viability, no alterations in acetyl-CoA levels were observed in orthovanadate challenged NC and DC (Table 3). Loss of cell viability, caused by orthovanadate, was accompanied by the concentration-dependent decrease in cell count, apparently resulting from their disintegration (Figs. 9–11). The relative extent of the cell loss was similar in both cell populations. By the end of 30 min incubation

Table 1
Thermodynamic parameters of the main phase transition of pure, fully hydrated DMPC multilamellar liposomes and DMPC/orthovanadate mixtures determined from heating and cooling scans collected at a heating (cooling) rate of 1 °C min^{-1}.

		Heating						Cooling					
		Pretransition			Main transition			Pretransition			Main transition		
		ΔH [kcal/mol]	ΔS [cal/K mol]	T_m [°C]	ΔH [kcal/mol]	ΔS [cal/K mol]	T_m [°C]	ΔH [kcal/mol]	ΔS [cal/K mol]	T_m [°C]	ΔH [kcal/mol]	ΔS [cal/K mol]	T_m [°C]
DMPC		0.7	2.0	14.9	5.5	18	24.4	0.4	1.0	9.4	5.5	19	23.5
Orthovanadate	+0.5 mM	0.6	2.0	14.8	5.0	17	24.4	nd	nd	nd	nd	nd	nd
	+1.0 mM												
	First	0.4	2.0	12.8	5.0	17	24.3	0.3	1.0	9.2	4.6	16	23.4
	Second	0.4	1.0	12.8	5.1	17	24.3	0.3	1.0	8.7	4.7	16	23.4

with 0.200 mmol/l concentration of Na_3VO_4, the total number of both NC and DC decreased by about 40–50% (Fig. 10).

Pyruvate dehydrogenase, aconitase and NADP-isocitrate dehydrogenase, energy producing enzymes, are known targets for inhibitory and degenerative effects of various neurotoxic metals [30]. Among them pyruvate dehydrogenase and aconitase appeared to be particularly sensitive to such inputs due to the presence of dihydrolipoate binding sites or non-heme, cysteine-bound iron in their active centers, respectively. Both cofactors may be displaced by various metals, yielding their inhibition or inactivation [30]. Incubation of harvested cells for 30 min with 0.200 mmol/l orthovanadate caused alterations in the pyruvate dehydrogenase complex and NADP-isocitrate dehydrogenase activities neither in NC nor in DC (Table 4). On the other hand, 30 min exposition of NC and DC to vanadate caused strong, concentration dependent inhibition of their aconitase with same Ki values equal to 0.0015 mmol/l (Fig. 12A, B). No correlation has been found between the decreases in aconitase activities in orthovanadate treated NC and DC and loss of their viability or structural integrity.

4. Discussion

Analyses by X-ray diffraction showed that 0.5 mM and higher concentrations of orthovanadate induced structural perturbations of the polar head group and the hydrophobic acyl regions of DMPE, whose bilayer structure completely collapsed with 1 mM Na_3VO_4. However, only very high concentrations of this compound (from 20 mM) were able to perturb to a low extent DMPC. These results can be explained on the basis of the different nature of DMPC and DMPE bilayers. Chemically the two lipids only differ in their terminal amino groups, these being $^{+}N(CH_3)_3$ in DMPC and $^{+}NH_3$ in DMPE. Moreover, both molecular conformations are very similar in their dry crystalline phases: their acyl chains are mostly parallel and extended with the polar groups lying perpendicularly to them; however, DMPE molecules pack tighter than those of DMPC, effect due to DMPE smaller polar group and higher effective charge [38]; as a consequence, water does not affect DMPE packing. On the other hand, gradual hydration of DMPC bilayers leads to water filling the highly polar interbilayer spaces. Consequently, there is an increase in its bilayer width from 54.5 Å when dry up to 64.5 Å when fully hydrated at a temperature below that of its main transition. This condition would have promoted the incorporation of vanadate ions into DMPC highly polar interbilayer space and the ensuing molecular perturbation of the phospholipid bilayer structure. However, this was not the case as amazingly DMPE bilayer was structurally perturbed by the orthovanadate. Somewhat similar results were observed with monomethylarsonate ions, which interacted with DMPE, but not with DMPC [44]. The explanation might lie in the fact that in both DMPE and DMPC the adjacent lipid molecules in the bilayer are held by electrostatic interactions and hydrogen bonds between neighboring amino and phosphate groups. Given DMPE smaller $^{+}NH_3$ groups, and therefore higher effectively charged than the bulkier $^{+}N(CH_3)_3$ of DMPC, orthovanadate ions preferentially interacted with DMPE. On the other hand, orthovanadate containing tetrahedrically coordinated V (V) is isostructural with orthophosphates and orthoarsenates [7,45], a property that allows it to inhibit enzyme activity by replacing phosphates as a substrate [7].

Table 2
Thermodynamic parameters of the main phase transition of pure, fully hydrated DMPE multilamellar liposomes and DMPE/orthovanadate mixtures determined from heating and cooling scans collected at a heating (cooling) rate of 1 °C min^{-1}.

	Heating			Cooling		
	ΔH [kcal/mol]	ΔS [cal/K mol]	T_m [°C]	ΔH [kcal/mol]	ΔS [cal/K mol]	T_m [°C]
DMPE						
First	6.7	21	50.7	6.0	19	49.2
Second	6.4	20	50.7	6.3	19	49.2
+Orthovanadate						
0.25 mM	6.5	21	50.5	6.08	22	48.1
0.50 mM	6.8	21	50.3	7.0	21	48.0
0.75 mM	7.0	22	50.1	7.1	22	47.9
1.00 mM						
First	6.9	22	49.7	7.2	23	47.8
Second	7.1	22	49.5	7.4	23	47.7

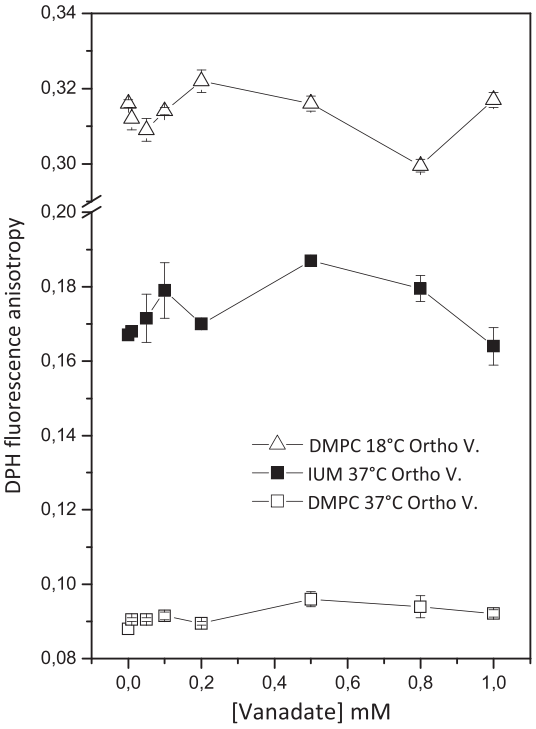

Fig. 4. Effect of orthovanadate on the anisotropy (r) of DPH embedded in DMPC LUV at 18 °C and 37 °C, and in isolated unsealed erythrocyte membranes (IUM) at 37 °C. Each point represents data average in duplicate and standard error.

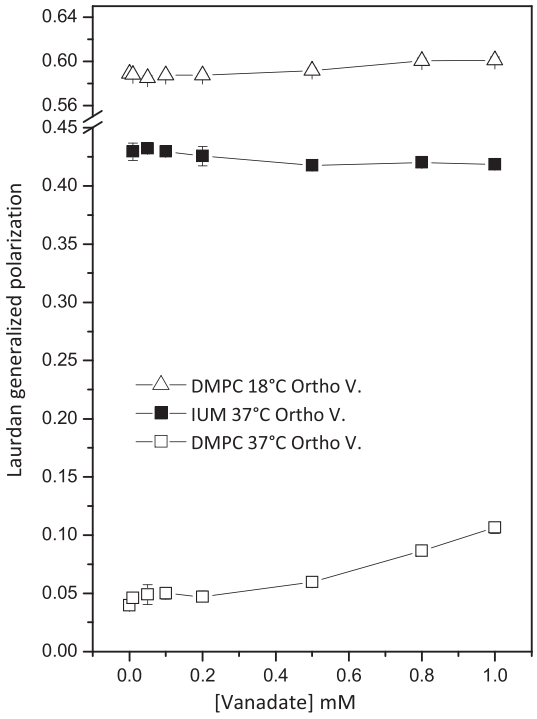

Fig. 5. Effect of orthovanadate on the generalized polarization (GP) of laurdan in DMPC LUV at 18 and 37 °C, and in isolated unsealed erythrocyte membranes (IUM) at 37 °C. Each point represents data average in duplicate and standard error.

The structural distinction between DMPC and its PE counterpart is related not only to the differences in lipid–lipid interaction and hydratation but also to hydrogen-bonding properties [46]. In DMPC bilayers, interfacial water molecules comprise the sole source of donor groups, that can hydrogen bond to the ester carbonyl groups, while in the case of hydrated DMPE bilayers other prospective source is the amine protons of the headgroup. During a stepwise hydration, the interfacial water molecules form H-bonds with the PO_2^- headgroup first and then with the C═O headgroups. However, only in the case of PCs, water molecules are assembled in the form of a clathrate hydration shell around the hydrophobic $N(CH_3)^{3+}$ group. Furthermore, exclusively for PEs, the amine hydrogens, form also H-bonds with the C═O group of the β chain of the same phospholipid molecule and the PO_2^- group of an adjacent phospholipid molecule. Apart from intermolecular, H-bonded water bridges link apposing PE bilayers, which prevent the interbilayer spacing from expanding.

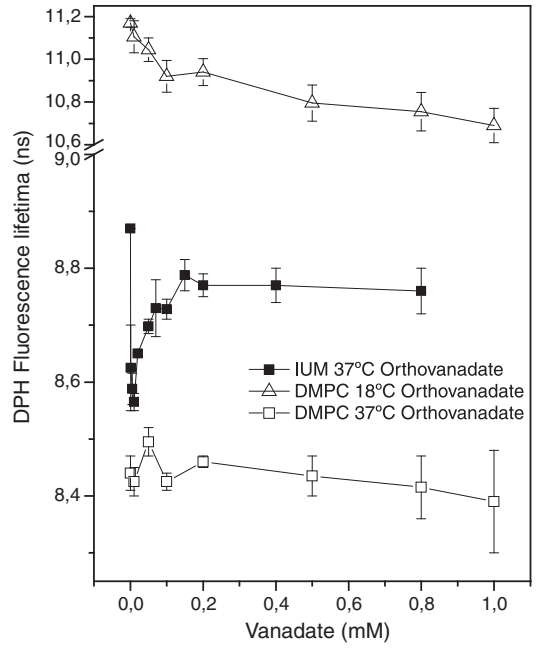

Fig. 6. Effect of orthovanadate on DPH fluorescence lifetime, in DMPC LUV at 18 and 37 °C, and in IUM at 37 °C. Lifetime distribution center obtained from the analysis is depicted as DPH lifetime (see Results). The errors represent the correlated 67% confidence limits of the reduced χ^2.

DSC data corroborate well with X-ray diffraction studies which showed that orthovanadate is capable of distortion of phospholipid thermal behavior. Similarly to arsenite we studied earlier [47] also in the case of orthovanadate the effect is much more pronounced for DMPE. Apparently, the transition temperature of DMPE is markedly higher than that of DMPC. This indicates that intermolecular interactions *via* hydrogen bonds, which are responsible for the higher T_m values of DMPE, also affect the transition entropy. In the liquid-crystalline phase DMPE seems to have slightly less motional freedom than DMPC, as verified by ^2H NMR measurements [48,49]. The changes detected by means of DSC for DMPC and DMPE bilayers in the presence of vanadium denote that it can interact with phospholipids in the form of orthovanadate and that the interaction mainly involves the external part of the hydrophobic core of the bilayer. In the DMPC/Na_3VO_4 system, the downshift of the pretransition temperature of 2.1 °C as well as its lowering even at as low content as 1 mol% confirmed the marked sensitivity to the presence of the foreign substance. Moreover, the more profound influence of orthovanadate on the pretransition (see Fig. 2 insert) is believed to demonstrate a stronger distortion of the DMPC packing in the gel state. On the contrary, both the insignificant T_m decrease and half-width of the peak ($\Delta T_{1/2}$) increase suggest that the hydrophobic core is poorly affected by vanadate molecules as they cannot insert deeply into the bilayer. Consequently, the interaction between vanadate and phospholipid is restricted mainly to the polar headgroup region. Undoubtedly, localization of foreign substances within the bilayer is of great importance when studying the interaction with membrane lipids. The parameter which can be regarded as an indicator of compound lipophilicity and solubility is the octanol–water partition coefficient (logP). When it is considered a logP value for orthovanadate of −3.268 [50], it is clear that this form shows a relatively low hydrophobicity. Evidently, the negative value of logP found for orthovanade is in accordance with X-ray and DSC results and seems to be a decisive factor for its effect on DMPE thermotropic phase behavior.

The impact of orthovanadate ions observed in our DSC studies can be ascribed to so-called Hofmeister mechanism reviewed in [51] and discussed in terms of indirect effects of the solute induced through changes in solvent properties. It has been shown [52,53] that some cosolutes, categorized as chaotropes, on increasing concentration, first lower the PC pretransition temperature and then suppress the pretransition. Moreover, they stabilize the fluid state of PC and PE bilayers, the latter effect being stronger for PE. With its four hydrogen bonding position, orthovanadate tends to disrupt the hydrogen-bonded water structure and accordingly, it can be classified as a chaotrope. A decrease of the T_m value in the concentration dependent manner that was observed in the presence of Na_3VO_4 may be due to a loosening of the hydrogen bonds network at the interface. This is in line with experimental data from spectrometry [54] and calorimetry [55] for DMPE showing downshift of T_m in the presence of different chaotropic in the range of 0.1–1 M.

Fluorescence measurement results indicate that orthovanadate addition induces small changes, predominantly in the hydrophobic domain of the lipid acyl chain of DMPC LUV and IUM bilayers. Laurdan GP significant changes only occurred in DMPC LUV in the liquid crystalline state; in fact, as a slight increase (Fig. 5) indicates that in this concentration interval orthovanadate elicited a small decrease in the dynamics of water molecules surrounding laurdan fluorophore during solvent relaxation following fluorophore excitation and/or water content at the glycerol

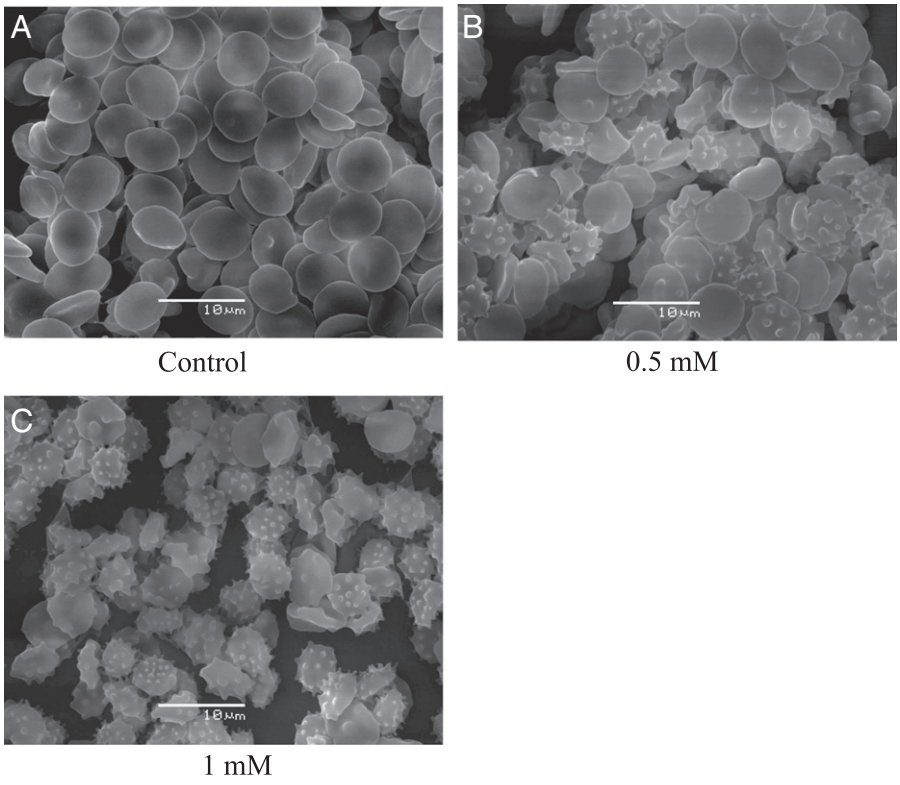

Fig. 7. Effects of orthovanadate on the morphology of human erythrocytes. SEM images of untreated erythrocytes (A), incubated with 0.5 mM (B), and 1 mM (C) of sodium orthovanadate.

backbone level of the bilayer. Changes in DPH fluorescence anisotropy (Fig. 4) suggest that orthovanadate elicits small changes in the lipid acyl chain packing order. The resemblance in the variation pattern of DMPC LUV at 37 °C and IUM, both in the liquid crystalline state suggests in turn that the effect of this additive depends on the lamellae phase state. DPH fluorescence lifetime is very sensitive to the environment polarity [56] which, in membrane bilayers, is considered to be determined by the local hydration at each depth due to the dynamic quenching by water. In this context, DPH fluorescence lifetime changes in IUM (Fig. 6) indicate that, at the depth of the membrane hydrophobic core, orthovanadate elicited a small although abrupt hydration increase since the first addition. This effect diminished at concentrations higher than 0.01 mM orthovanadate, possible due to the interactions of the latter with water molecules present in small numbers. We hypothesize that the presence of proteins induces the appearance of interfaces between the lipids and protein surfaces, which can be considered as a defect when compared with a pure lipid phase. Ho and Stubbs [57] provided the first evidence for the existence of water at the protein–lipid hydrophobic interface. These membranes, due to the high content of proteins [58], have a large amount of this type of interfaces and, therefore in close proximity with lipid domains. So, DPH is able to detect hydration changes in these interfaces caused by orthovanadate in the lowest concentration range.

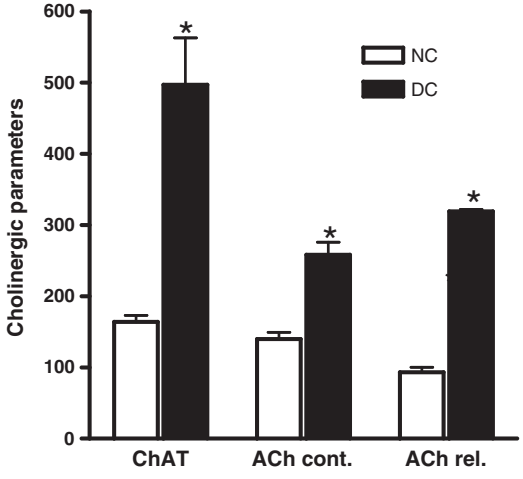

Fig. 8. Effect of cAMP/retinoic acid induced differentiation on choline acetyltransferase (ChAT, pmol/min/mg protein), acetylcholine content (ACh cont., pmol/mg protein) and acetylcholine release (ACh rel., pmol/min/mg protein) in SN56 cholinergic neuroblastoma cells. Data are means ± SEM from 6 experiments. Significantly different from non-differentiated cells, *$p < 0.001$.

According to the bilayer couple hypothesis [59,60], shape changes are induced in red cells due to the insertion of foreign species in either outer or inner monolayer of the erythrocyte membrane. Thus, spiculated shapes (echinocytes) are observed in the first case while cup shapes (stomatocytes) are produced in the second due to the differential expansion of the corresponding monolayer. Given the extent of the interaction of orthovanadate ions with DMPE, class of lipid preferentially located in the inner monolayer of the erythrocyte membrane, stomatocytes were expected from erythrocytes incubated with Na_3VO_4. SEM examination of specimens showed that in fact echinocytes were observed. These results might imply that orthovanadate preferentially interacted with proteins located into the outer monolayer of the erythrocyte membrane. In fact, vanadate interactions with several proteins have been reported [2,3,7]. Considering the high protein content of this membrane, it must have a large amount of lipid–protein interfaces, so small protein conformational changes induced by vanadate could influence on membrane properties.

Also in neuronal cells orthovanadate caused apparent membrane malformations (Fig. 9). They however, might result from combination its direct binding with plasma membrane proteolipids and secondary alterations resulting from disturbed energy metabolism (Figs. 2, 3, 5, 7, 9, 11, 12). Concentrations of orthovanadate used in this study

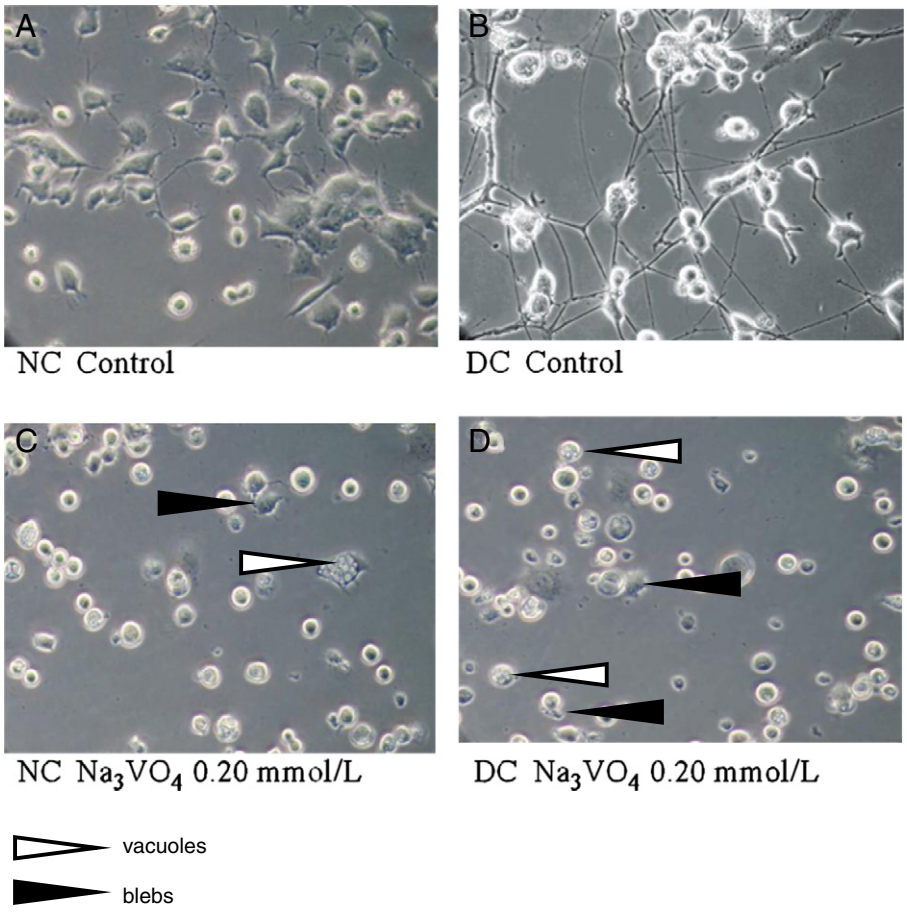

Fig. 9. Effect of orthovanadate on morphology of nondifferentiated (A, C) and differentiated (B, D) SN56 cholinergic neuroblastoma cells. Data are representative for 3 experiments. Membrane blebs, black arrows; vacuoles, white arrows.

that displayed apparent neurotoxic effects were lower than elementary vanadium concentrations applied, in form of inorganic salts either *in vivo* or in cell culture studies, by other investigators [20,61,62]. Differentiated and nondifferentiated phenotypes of septal cholinergic neuronal cells were used (Figs. 8 and 9) to assess to what degree increased acetyl-CoA consumption for acetylcholine synthesis in the former affects their susceptibility to apparently neurotoxic vanadate compounds (Fig. 8) [20,30,61]. Our past studies have shown that cholinergic cells with high expression of the cholinergic phenotype were more susceptible to vast range of neurotoxins, like aluminum, zinc, amyloid-beta or NO excess, than those with low level of cholinergic metabolism [30,63]. Such differential susceptibility to neurodegenerative insults was

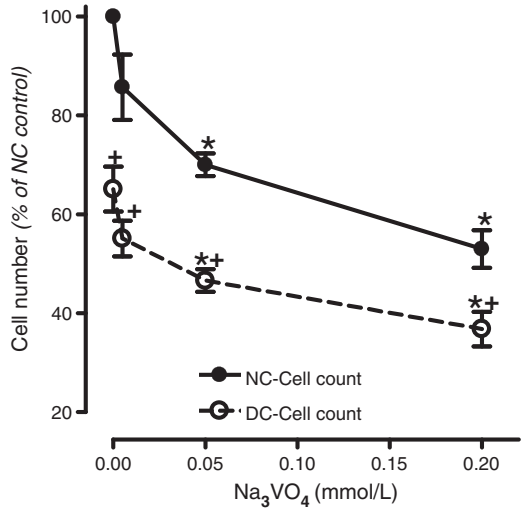

Fig. 10. Concentration dependent, short-term effects of orthovanadate on number of nondifferentiated (NC) and differentiated (DC) SN56 cholinergic neuroblastoma cells. Data are means ± SEM from 4 experiments. Significantly different from no orthovanadate control, *p<0.01; respective NC group, $^{+}$p<0.05.

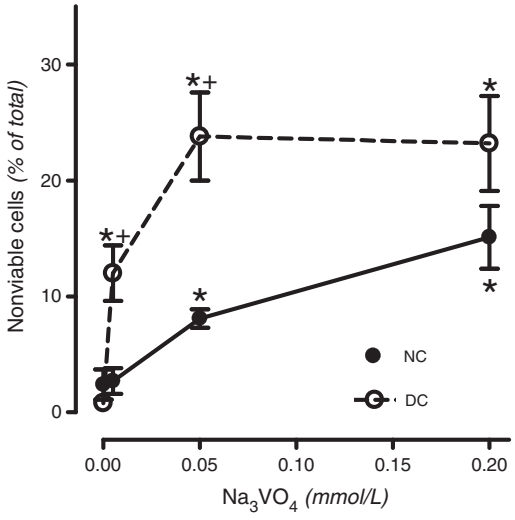

Fig. 11. Concentration dependent, short-term effects of orthovanadate on nonviable-trypan blue positive fraction of nondifferentiated (NC) and differentiated (DC) SN56 cholinergic neuroblastoma cells. Data are means ± SEM from 4 experiments. Significantly different from no orthovanadate control, *p<0.01; respective NC group, $^{+}$p<0.05.

Table 3
Effect of orthovanadate on acetyl-CoA content in cholinergic SN56 neuroblastoma cells.

Addition Na_3VO_4 (mmol/l)	Nondifferentiated cells	Differentiated cells
	Whole cell acetyl-CoA (pmol/mg protein)	
Control	23.3 ± 2.0	22.0 ± 0.9
0.005	25.9 ± 1.5	20.8 ± 2.1
0.050	21.7 ± 2.8	21.2 ± 1.5
0.200	23.6 ± 2.1	23.5 ± 1.4

Data are means ± SEM from four experiments.

concluded to result from relative shortage of acetyl-CoA for energy production due to its greater utilization for acetylcholine synthesis in DC. Data presented here support this hypothesis as orthovanadate, in low or moderate concentrations within short 30 min time caused a differential loss of the cell viability that was significantly greater in DC than in NC (Figs. 10 and 11). This differential orthovanadate cytotoxicity to NC and DC cannot be explained by the inhibition of aconitase as it was equally strong (Ki 0.0015 mmol/l) in both experimental groups (Fig. 12A, B). This could impair the energy production due to inhibition of metabolic flow through the entire TCA on the level of aconitase step. The mechanism of this inhibition remains elusive. It may be supposed that vanadate could remove iron from S-Fe non heme clusters in the enzyme active center by the formation of Fe-orthovanadate complexes [64–66]. This inhibitory effect was similar to those exerted by Zn, Al and NO known to interfere with aconitase active site [30,64]. The specificity of this interaction is supported by the fact that the other enzymes of energy metabolism: pyruvate dehydrogenase complex (component E3) with lipoamide binding sites and NADP-isocitrate dehydrogenase, with NADP binding domain appeared to be resistant to orthovanadate (Tables 3 and 4). However, these finding themselves do not explain highly differential susceptibility of DC and NC to orthovanadate, as its inhibitory affinities to aconitase were similar in both cell groups (Figs. 11 and 12). Thus, greater than NC susceptibility of DC to orthovanadate could result from greater energy expenditures and acetyl-CoA shortages in their mitochondria connected with supporting higher rates of acetylcholine metabolism (Fig. 8) [30,64].

Vanadium concentrations in blood of non-exposed humans to this trace element were found to be in the range of 0.05–0.10 μmol/l but it could rise up to 10,000 times in highly exposed persons [67,68]. On the other hand, vanadate levels in human fetal brains were equal to about 1 μmol/l, indicating the existence of uptake mechanisms for vanadate compounds in the brain [69]. It indicates that blood–brain barrier effectively prevents brain overload with this metal. Nevertheless, the Ki for orthovanadate 0.0015 mmol/l to aconitase (Fig. 12B), corresponds to the brain vanadium levels in exposed animals equal to 0.002 mmol/l [70]. Therefore, this *in vitro* effect may be of pathophysiological importance. It is important to stress that blood parameters showed little or no reflection of toxicity after a long-term supplementation of vanadium compounds, which might be due to the brisk transport of vanadium from blood to the tissues [2]. However, the lethal concentration of vanadium in the blood of a patient was calculated to be about 0.12 mM [71]. It corresponds well with gross cell membrane changes seen in erythrocyte and neuronal membranes at 0.1–0.2 mM orthovanadate concentrations in the extracellular space (Figs. 7 and 10).

Table 4
Short-term effects of sodium orthovanadate on activities of selected mitochondrial enzymes in SN56 cholinergic neuroblastoma cells.

Enzyme		Na_3VO_4 added (mmol/l)			
		Enzyme specific activity (nmol/min/mg protein)			
		Control	0.005	0.100	0.200
Pyruvate dehydrogenase	NC	7.76 ± 0.23	7.68 ± 0.26	6.98 ± 0.97	7.11 ± 0.45
	DC	8.93 ± 0.70	8.47 ± 0.14	7.76 ± 0.38	8.85 ± 0.44
NADP isocitrate dehydrogenase	NC	26.3 ± 0.9	27.4 ± 0.2	27.5 ± 0.7	28.3 ± 0.4
	DC	27.5 ± 0.9	28.0 ± 1.6	30.1 ± 1.9	30.2 ± 2.6

Data are means ± SEM from four experiments.

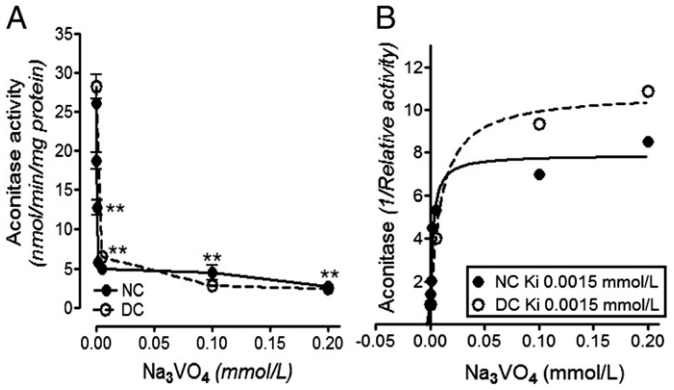

Fig. 12. Concentration dependent, short-term effects of orthovanadate (A) on aconitase activity in nondifferentiated (NC) and differentiated (DC) SN56 cholinergic neuroblastoma cells. Dixon's plots for Ki for orthovanadate (B). Data are means ± SEM from 3 to 6 experiments. Significantly different from no orthovanadate control, $^{**}p<0.01$.

Acknowledgements

Work was supported by FONDECYT (1090041), MNSW (IP 2010 035370 and NN401 0299 37) and GUMed fund St-57. Calorimetric measurements were carried out using the instrument purchased thanks to financial support of European Regional Development Fund (contract No. POIG.02.01.00-12-167/08, project Malopolska Centre of Biotechnology).

References

[1] D.G. Barceloux, Vanadium, Clin. Toxicol. 37 (1999) 265–278.
[2] B. Mukherjee, B. Patra, S. Mahapatra, P. Banerjee, A. Tiwari, M. Chatterjee, Vanadium — an element of atypical biological significance, Toxicol. Lett. 150 (2004) 135–143.
[3] A. Sakai, Orthovanadate, an inhibitor of protein tyrosine phosphatases, acts more potently as a promoter than as an initiator in the BALB/3T3 cell transformation, Carcinogenesis 18 (1997) 1395–1399.
[4] A. Scibor, H. Zaporowska, Effects of combined vanadate and magnesium treatment on erythrocyte antioxidant defense system in rats, Environ. Toxicol. Pharmacol. 30 (2010) 153–161.
[5] J.J. Rodríguez-Mercado, M.A. Altamirano-Lozano, Vanadio, contaminación, metabolismo y genotoxicidad, Rev. Int. Contam. Ambient 22 (2006) 173–189.
[6] X. Yang, K. Wang, J. Lu, D.C. Crans, Membrane transport of vanadium compounds and the interaction with the erythrocyte membrane, Coord. Chem. Rev. 237 (2001) 103–111.
[7] J.E. Benabe, L.A. Echegoyen, B. Pastrana, M.M. Maldonado, Mechanism of inhibition of glycolysis by vanadate, J. Biol. Chem. 262 (1987) 9555–9580.
[8] S.L. Schrier, I. Junga, L. Ma, Studies on the effects of vanadate on endocytosis and shape changes in human red blood cells and ghosts, Blood 68 (1986) 1008–1014.
[9] G.R. Hogan, Comparative erythropoietic effects of three vanadium compounds, Sci. Total Environ. 256 (2000) 185–189.
[10] H. Zaporowska, W. Wasilewski, Haematological effects of vanadium on living organisms, Comp. Biochem. Physiol. C 102 (1992) 223–231.
[11] H. Zaporowska, W. Wasilewski, Haematological results of vanadium intoxication in wistar rats, Comp. Biochem. Physiol. C 101 (1992) 57–61.
[12] J.M. Boon, B.D. Smith, Chemical control of phospholipid distribution across bilayer membranes, Med. Res. Rev. 22 (2000) 251–281.
[13] P.F. Devaux, A. Zachowsky, Maintenance and consequences of membrane phospholipids asymmetry, Chem. Phys. Lipids 73 (1994) 107–120.
[14] M. Suwalsky, R. Castro, F. Villena, C.P. Sotomayor, Cr(III) exerts stronger structural effects than Cr(VI) on the human erythrocyte membrane and molecular models, J. Inorg. Biochem. 102 (2008) 842–849.
[15] M. Suwalsky, F. Villena, C.P. Sotomayor, Mn^{2+} exerts stronger structural effects than the Mn-citrate complex on the human erythrocyte membrane and molecular models, J. Inorg. Biochem. 104 (2010) 55–61.
[16] M. Suwalsky, C. Rivera, F. Villena, C.P. Sotomayor, Toxic effects of arsenic on human erythrocytes, in: N. Kabai, et al., (Eds.), The Global Arsenic Problem: Challenges for Safe Water Production, Ch. 3, CRC Press, Boca Raton, FL, 2010, pp. 37–46.
[17] A. Jankowska-Kulawy, S. Gul-Hinc, H. Bielarczyk, J.B. Suszkiw, T. Pawełczyk, A. Dyś, A. Szutowicz, Effects of lead on cholinergic SN56 neuroblastoma cells, Acta Neurobiol. Exp. 68 (2008) 1–10.

[18] Z. Liu, P. Li, D. Zhao, H. Tang, J. Guo, Protection by vanadium, a contemporary treatment approach to both diabetes and focal cerebral ischemia in rats, Biol. Trace Elem. Res. 145 (2012) 66–70.
[19] Y. Shechter, Insulin-mimetic effects of vanadate. Possible implications for future treatment of diabetes, Diabetes 39 (1990) 1–5.
[20] H.A. Ngwa, A. Kanthasamy, V. Anantharam, C. Song, T. Witte, R. Huk, A.G. Kanthasamy, Vanadium induces dopaminergic neurotoxicity via protein kinase Cdelta dependent oxidative signaling mechanisms: relevance to etiopathogenesis of Parkinson's disease, Toxicol. Appl. Pharmacol. 240 (2009) 273–285.
[21] F. Han, N. Shioda, S. Moriguchi, Z.H. Qin, K. Fukunaga, The vanadium (IV) compound rescues septo-hippocampal cholinergic neurons from neurodegeneration in olfactory bulbectomized mice, Neuroscience 151 (2008) 671–679.
[22] N. Shioda, T. Ishigami, F. Han, S. Moriguchi, M. Shibuya, Y. Iwabuchi, K. Fukunaga, Activation of phosphatidylinositol 3-kinase/proteion kinaseB pathway by a vanadyl compound mediates its neuroprotective effect in mouse brain ischemia, Neuroscience 148 (2007) 221–229.
[23] T. Parasassi, E. Gratton, Membrane lipid domains and dynamics as detected by Laurdan fluorescence, J. Fluoresc. 5 (1995) 59–69.
[24] J.R. Lakowicz, Principles of Fluorescence Spectroscopy, Plenum, New York, 1999.
[25] T. Parasassi, G. Destasio, G. Ravagnan, R.M. Rusch, E. Gratton, Quantitation of lipid phases in phospholipid-vesicles by the generalized polarization of Laurdan fluorescence, Biophys. J. 60 (1991) 179–189.
[26] R.D. Spencer, G. Weber, Measurement of subnanosecond fluorescence lifetimes with a cross-correlation phase fluorometer, Ann. N. Y. Acad. Sci. 158 (1969) 361–376.
[27] E. Gratton, D. Jameson, R.D. Hall, Multifrequency phase and modulation fluorometry, Annu. Rev. Biophys. Bioeng. 13 (1984) 105–124.
[28] J.T. Dodge, C. Mitchell, C.D. Hanahan, The preparation and chemical characterization of haemoglobin-free ghosts of human erythrocytes, Arch. Biochem. Biophys. 100 (1963) 119–130.
[29] D.N. Hammond, H.J. Lee, J.H. Tonsgard, B.H. Wainer, Development and characterization of clonal cell lines derived from septal cholinergic neurons, Brain Res. 512 (1990) 190–200.
[30] A. Szutowicz, H. Bielarczyk, S. Gul, A. Ronowska, T. Pawełczyk, Phenotype-dependent susceptibility of cholinergic neuroblastoma cells to neurotoxic inputs, Met. Brain Dis. 21 (2006) 149–161.
[31] A. Szutowicz, H. Bielarczyk, Elimination of CoASH interference from acetyl-CoA assay by maleic anhydride, Anal. Biochem. 164 (1987) 292–296.
[32] J. Wang, P.S. Green, W. Simpkins, Estradiol protects against ATP depletion, mitochondrial membrane potential decline and generation of reactive oxygen species induced by 3-nitropropionic acid in SK-N-SH human neuroblastoma cells, J. Neurochem. 77 (2001) 804–811.
[33] F. Fonnum, A rapid radiochemical method for the determination of choline acetyltransferase, J. Neurochem. 24 (1975) 407–409.
[34] A. Szutowicz, M. Stepien, G. Piec, Determination of pyruvate dehydrogenase and acetyl-CoA synthetase activities using citrate synthase, Anal. Biochem. 115 (1981) 81–87.
[35] G.W.E. Plaut, Isocitric dehydrogenase (TPN-linked) from pig heart (revised procedure), in: S.P. Colowick, N.O. Kaplan (Eds.), Methods in Enzymology, vol. 5, Academic Press, New York, 1962, pp. 645–651.
[36] J.J. Villafranca, The mechanism of aconitase action: evidence for an enzyme isomerization by studies of inhibition by tricarboxylic acids, J. Biol. Chem. 249 (1974) 6149–6155.
[37] M. Bradford, A rapid sensitive method for the quantitation of microgram quantities of protein utilizing the principle of protein-dye binding, Anal. Biochem. 72 (1976) 248–254.
[38] M. Suwalsky, Phospholipid bilayers, in: J.C. Salamone (Ed.), Polymeric Materials Encyclopedia, CRC, Boca Raton, FL, 1996, pp. 5073–5078.
[39] D. Marsh, Analysis of the chain length dependence of lipid phase transition temperatures: main and pretransitions of phosphatidylcholines; main and nonlamellar transitions of phosphatidylethanolamines, Biochim. Biophys. Acta 1062 (1991) 1–6.
[40] C. Huang, S. Li, Calorimetric and molecular mechanics studies of the thermotropic phase behavior of membrane phospholipids, Biochim. Biophys. Acta 1422 (1999) 273–307.
[41] R. Koynova, M. Caffrey, Phases and phase transitions of the phosphatidylcholines, Biochim. Biophys. Acta 1376 (1998) 91–145.
[42] N.A.H. Lewis, R.N. McElhaney, Calorimetric and spectroscopic studies of the polymorphic phase behaviour of a homologous series of n-saturated 1,2-diacyl phosphatidylethanolamines, Biophys. J. 64 (1993) 1081–1096.
[43] A. Szutowicz, Aluminum, NO and nerve growth factor neurotoxicity in cholinergic neurons, J. Neurosci. Res. 66 (2001) 1009–1018.
[44] M. Suwalsky, C. Rivera, C.P. Sotomayor, M. Jemiola-Rzeminska, K. Strzalka, Monomethylarsonate (MMA^{V}) exerts stronger effects than arsenate on the structure and thermotropic properties of phospholipids bilayers, Biophys. Chem. 132 (2008) 1–8.
[45] A.F. Wells, Structural Inorganic Chemistry, Oxford, London, Great Britain, 1962.
[46] J.M. Boggs, Lipid intermolecular hydrogen bonding: influence on structural organization and membrane function, Biochim. Biophys. Acta 906 (1987) 353–404.
[47] M. Suwalsky, C. Rivera, F. Villena, C.P. Sotomayor, M. Jemiola-Rzeminska, K. Strzalka, Arsenite interaction with phospholipid bilayers as molecular models for the human erythrocyte membrane, Biophys. Chem. 127 (2007) 28–35.
[48] A. Blume, D.M. Rice, R.J. Wittebort, R.G. Griffin, Molecular dynamics and conformation in the gel and liquid-crystalline phases of phosphatidylethanolamine bilayers, Biochemistry 21 (1982) 6220–6230.
[49] D. Marsh, A. Watts, I.C.P. Smith, Dynamic structure and phase behaviour of dimyristoylphosphatidylethanolamine bilayers studied by deuterium nuclear magnetic resonance, Biochemistry 22 (1983) 3023–3026.
[50] http://www.chemexper.com/chemicals/supplier/cas/137. (Retrieved on February 29, 2012).
[51] M.G. Cacace, E.M. Landau, J.J. Ramsden, The Hofmeister series: salt and solvent effects on interfacial phenomena, Q. Rev. Biophys. 30 (1997) 241–277.
[52] R. Bartucci, S. Belsito, L. Sportelli, Neutral lipid bilayers interacting with chaotropic anions, Chem. Phys. Lipids 79 (1996) 171–180.
[53] R. Koynova, J. Brankov, B. Tenchov, Modulation of lipid phase behaviour by kosmotropic and chaotropic solutes, Eur. Biophys. J. 25 (1997) 261–274.
[54] M. Kodama, H. Inoue, Y. Tsuchida, The behavior of water molecules associated with structural changes in phosphatidylethanolamine assembly, Thermochim. Acta 266 (1995) 373–384.
[55] E.S. Rowe, Thermodynamic reversibility of phase transitions. Specific effects of alcohols on phosphatidylcholines, Biochim. Biophys. Acta 813 (1985) 321–330.
[56] C. Zannoni, A. Argioni, P. Cavatorta, Fluorescence depolarization in liquid crystals and membrane bilayers, Chem. Phys. Lipids 32 (1983) 179–250.
[57] C. Ho, C.D. Stubbs, Hydration at the membrane protein–lipid interface, Biophys. J. 63 (1992) 897–902.
[58] D.B. Data, Membrane Biochemistry, Floral Publishing, Madison, WI, 1987.
[59] M.P. Sheetz, S.J. Singer, Biological membranes as bilayer couples. A molecular mechanism of drug–erythrocytes interactions, Proc. Natl. Acad. Sci. U.S.A. 71 (1974) 4457–4461.
[60] G. Lim, M. Wortis, R. Mukhopadhyay, Stomatocyte–discocyte–echinocyte sequence of the human red blood cell: evidence for the bilayer-couple hypothesis from membrane mechanics, Proc. Natl. Acad. Sci. U.S.A. 99 (2002) 16766–16769.
[61] G.B. Garcia, M.E. Biancardi, A.D. Quiroga, Vanadium (V)-induced neurotoxicity in the rat central nervous system: a histo-immunohistochemical study, Drug Chem. Toxicol. 28 (2005) 329–344.
[62] S.S. Haider, A.A. Abdel-Gayoum, M. El-Fakhiri, K.M. Ghwarsha, Effect of selenium on vanadium toxicity in different regions of rat brain, Hum. Exp. Toxicol. 17 (1998) 23–28.
[63] A. Jankowska, B. Madziar, M. Tomaszewicz, A. Szutowicz, Acute and chronic effects of aluminum on acetyl-CoA and acetylcholine metabolism in differentiated and nondifferentiated SN56 cholinergic cells, J. Neurosci. Res. 62 (2000) 615–622.
[64] A. Ronowska, S. Gul-Hinc, H. Bielarczyk, T. Pawełczyk, A. Szutowicz, Effects of zinc on SN56 cholinergic neuroblastoma cells, J. Neurochem. 103 (2007) 972–983.
[65] G.L. Sillen, Stability Constants of Metal-Ion Complexes, Suppl. 1, Part 1, in: G.L. Sillen (Ed.), Special Publication, No 25, Chemical Society, Burlington House, London, 1971.
[66] B. Sreedhar, K.M. Nair, Modulation of aconitase, metallothionein, and oxidative stress in zinc deficient rat intestine during zinc and iron repletion, Free Radic. Biol. Med. 39 (2005) 999–1008.
[67] V.A. Granadillo, J.E. Tahan, O. Salgado, L.E. Elejalde, B. Rodriguez-Iturbe, G.B. Romero, R.A. Romero, The influence of the blood levels of lead, aluminum and vanadium upon the arterial hypertension, Clin. Chim. Acta 233 (1995) 47–59.
[68] J. Kucera, A.R. Byrne, A. Mravcova, J. Lener, Vanadium levels in hair and blood of normal and exposed persons, Sci. Total Environ. 115 (1992) 191–205.
[69] J.E. Tahan, L.C. Barrios, L. Marcano, V.A. Granadillo, H.S. Gubillan, J.M. Sanchez, M.C. Rodriguez, O. Salgado, R.A. Romero, Levels of Hg, Pb and V in brain, kidney, liver and lung of anencephalic fetuses from the Eastern coast of Lake Maracaibo, Venezuela, Trace Elem. Electrolytes 13 (1996) 7–13.
[70] A.L. Edel, M. Kopilas, T.A. Clark, F. Aguilar, P.K. Ganguly, C.E. Heyliger, G.N. Pierce, Short-term bioaccumulation of vanadium when ingested with a tea decoction in streptozotocin-induced diabetic rats, Metabolism 55 (2006) 263–270.
[71] B. Boulassel, N. Sadeg, O. Roussel, M. Perrin, H. Belhadj-Tahar, Fatal poisoning by vanadium, Forensic Sci. Int. 206 (2011) e79–e81.